University of Bath

Grice, J.R., Taylor, P.H., Eatock Taylor, R., Zang, Z. and Walker, D.A.G.

Extreme free surface elevations beneath offshore platforms, second order trapping, and the near flat form of the quadratic transfer functions.

Extreme wave elevations beneath offshore platforms, second order trapping, and the near flat form of the quadratic transfer functions

J.R. Grice[a], P.H. Taylor[a], R. Eatock Taylor[a], J. Zang[b], D.A.G. Walker[c]

[a]*Department of Engineering Science, University of Oxford, Parks Road, Oxford, OX1 3PJ, UK*
[b]*Department of Architecture and Civil Engineering, University of Bath, Bath, BA2 7AY, UK*
[c]*BP Exploration Operating Co. Ltd, Chertsey Road, Sunbury-on-Thames, TW16 7LN, UK*

Abstract

Extreme free surface elevations due to wave-structure interactions are investigated to second order using Quadratic Transfer Functions (QTFs). The near-trapping phenomenon for small arrays of closely spaced columns is studied for offshore applications, and the excitation of modes by linear and second order interactions is compared. A simple method for approximating near-trapped mode shapes is shown to give good results for both linear and second order excitation. Low frequency near-trapped mode shapes are shown to be very similar whether excited linearly or to second order. Approximating surface elevation sum QTF matrices as being flat perpendicular to the leading diagonal is investigated as a method for greatly reducing lengthy QTF calculations. The effect of this approximation on second order surface elevation calculations is assessed and shown to be reasonably small with realistic geometries for semi-submersible and tension-leg platforms.

*Corresponding author. Tel.: +447990500027; E-mail: jamesgrice23@gmail.com

1. Introduction

The phenomenon of near-trapping is a near-resonant local response excited by free-surface waves of a certain frequency interacting with arrays of obstacles such as vertical surface-piercing columns (see Linton and Evans (1993), Evans et al. (1994), and Evans and Porter (1997)) or with other geometries, including single bodies. Each near-trapping frequency is associated with a mode of strong local free surface oscillation which decays rather slowly in time due to wave radiation to infinity. However, the excitation periods of all but the lowest one or two near-trapped modes are usually too short to be significantly excited linearly by typical storm waves for most multi-column bodies as large as semi-submersible or tension-leg platforms. Non-linear wave responses can arise from various effects, such as the velocity squared term in the Bernoulli equation for pressure, and other non-linearities in the free surface boundary condition. The lowest order non-linear force is at sum and difference combination frequencies of the component incident wave frequencies. Second order sum frequency excitation of the higher near-trapped modes by waves with an incident period twice as long as the mode excitation period can form a large component of extreme wave-structure interactions (Walker et al. (2008), Grice (2013)). Since second order responses can cause such a large contribution to the overall surface elevation, linear calculations are not sufficient to accurately model extreme wave-structure interactions. One must include second order contributions, despite the large increase in computational complexity, and the use of quadratic transfer functions (QTFs) is one possible method of modelling the second order responses in real sea-states. Quadratic transfer functions (defined below) are convolved with the incident surface elevation spectrum to give the response surface elevation spectrum, using the standard Volterra series approach described, for example, by Schetzen (1980).

1.1. Transfer functions

Potential flow theory is used here to describe the incident waves, and the wave scattering by the structure. The unknown velocity potential, satisfying

2

a non-linear boundary condition, is expressed as a perturbation expression in wave steepness, truncated at the second order terms (i.e. terms quadratic in wave amplitude). Equation 1 describes the linear response elevation $\eta_R^{(1)}$ to two incident waves with amplitude A_i m, angular frequency ω_i rad/s, and phase ψ_i rad, where $i = 1, 2$ and b_i is the linear transfer function (LTF) at frequency ω_i. The second order response components are then given by Equation 2 with the QTFs for the potential sum term b_{PS}, quadratic sum term b_{QS}, potential difference term b_{PD}, and quadratic difference term b_{QD}. This decomposition into quadratic and potential terms has been widely used by others to facilitate interpretation and verification of computed results (see, for example, early examples in Kim and Yue (1990) and Eatock Taylor (1991).) The quadratic terms refer to the simple local product of two first order incident wave components. Potential terms arise from the inhomogeneous equations for the fluid velocity potential at second order and are driven by the interactions between pairs of incident frequency components. These are associated with the generation and propagation of free waves out to infinity as well as local contributions close to the structure. Sum terms refer to response at a frequency equal to the sum of the incident frequencies, $\omega_R = \omega_i + \omega_j$, (i.e. double the incident frequency for the self-interaction) and the difference terms refer to a response at $\omega_R = \omega_i - \omega_j$.

$$\eta_R^{(1)} = b_1\eta_1 + b_2\eta_2 = \Re\{b_1 A_1 e^{-i(\omega_1 t + \psi_1)} + b_2 A_2 e^{-i(\omega_2 t + \psi_2)}\} \tag{1}$$

$$\eta_R^{(2)} = \Re\{(b_{PS} + b_{QS})A_1 A_2 e^{-i((\omega_1 + \omega_2)t + \psi_1 + \psi_2)}\}$$
$$+ \Re\{(b_{PD} + b_{QD})A_1 A_2 e^{-i((\omega_1 - \omega_2)t + \psi_1 - \psi_2)}\} \tag{2}$$

Here $\Re$ indicates that the real part is taken.

The quadratic transfer functions (QTFs) can be found using boundary element potential flow codes such as WAMIT (see Lee et al. (1991) and Newman and Lee (1992)) or the Oxford code DIFFRACT (see Eatock Taylor and Chau (1992), Zang et al. (2006), and Eatock Taylor et al. (2008)). These lead to

3

the total surface elevation to second order in the vicinity of a structure for a given incident wave. Calculation of QTFs can be very computationally intensive and so it would be beneficial if a reasonable approximation could be found which reduced the number of QTF calculations necessary. Linear calculations are quick and cheap but have been shown to be insufficient when modelling extreme wave structure interactions, see for example Walker et al. (2008) and Stansberg (2014). Calculation of each QTF not only takes much longer than for LTFs, but for an incident wave surface elevation spectrum with N frequency components one needs to fill four $N \times N$ matrices to cover the second order interactions between all possible pairs of frequency components. Use of symmetry when populating each matrix of QTFs can be used to reduce the number of calculations from N^2 to $N(N + 1)/2$ (the leading diagonal plus one side) but this is still computationally expensive.

Taylor et al. (2007) introduced a near-flat sum QTF matrix approximation for surface elevation around cylinder arrays. The authors observed that at low frequencies the sum QTF is a strong function of the output frequency ($\omega_S = \omega_i + \omega_j$) and virtually independent of the frequency difference ($\omega_D = \omega_i - \omega_j$), which is the distance away from the leading diagonal. This observation means that the whole QTF matrix might be approximated using only the leading diagonal. It would allow a reduction of the number of QTF calculations from $N(N+1)/2$ to N. This observation has the same empirical form as the Newman (1974) approximation for difference frequency forces in vessels in irregular waves but Taylor et al. showed that a similar form of approximation is possible in second order sum surface elevation QTFs for arrays of cylinders. This approximation is investigated further to assess whether it is reasonable for use in wave-structure interaction analysis for certain types of configuration such as semi-submersible and tension leg platforms.

2. Near-trapped modes

Before beginning the lengthy process of calculating quadratic surface elevation transfer functions it is important to investigate the incident frequencies most likely to give a violent response. By finding the near-trapped mode frequencies for a given structure one can then plan the frequencies at which transfer functions should be calculated to give a reasonable model of extreme wave-structure interactions. The structure under study here is a simplified version of a typical large offshore platform. It consists of four vertical bottom-seated circular columns of radius a=12.34 m, in water of depth 30 m, and with centres located at $(\pm41.42\text{ m}, \pm41.42\text{ m})$. Figure 1(a) shows the mesh for this simplified four circular column model and Figure 1(b) shows the boundary mesh for a more realistic offshore structure. Only one quadrant is shown, as two planes of symmetry are assumed to minimise computation time. Analysis with the mesh in Figure 1(b) will be discussed later. To identify the near-trapped frequencies for the simplified structure in Figure 1(a) the method of Linton and Evans (1990) was used, leading to thirteen near-trapped modes with a wavenumber less than 0.3 m^{-1}. Open ocean wave components with wavenumbers greater than this would have minimal energy and are therefore not considered.

(a) Simple mesh for four circular columns
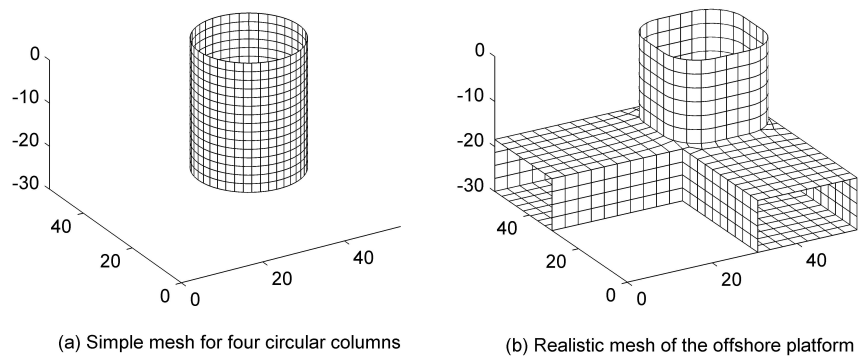
(b) Realistic mesh of the offshore platform

Figure 1: Examples of the meshes used in Sections 2 (Figure (a)) and 3 (Figure (b)).

It is also possible to identify complex wavenumbers at which theoretically a

5

phenomenon of pure trapping occurs (with no radiation of waves away from the body). The method of Linton and Evans (1990) makes use of a truncated infinite Fourier-Bessel series to model the total wave field including wave-structure interactions. When the matrix of coefficients associated with this truncated infinite series has a value of the determinant close to zero, a particularly violent response can occur. If a wavenumber leading to a zero in this determinant is real then pure-trapping has occurred. However, this only occurs for particular special geometries. In contrast, a much wider range of geometries leads to the phenomenon of near-trapped modes. The wavenumbers leading to zeros in the determinant are often complex and near-trapping may be thought of as the situation closest to pure-trapping if one sets the imaginary part of these complex wavenumbers to zero. The size of the imaginary part gives a measure of the wave damping due to radiation to infinity. The modes with the smallest imaginary wavenumber components are closest to pure-trapping with rather weak radiation leaking out to infinity and are therefore likely to have very large responses when excited by incoming waves. Detailed discussion on the linear excitation of these near-trapped modes for the same structure as considered here is given in Section 3 of Grice et al. (2013). A list of the predicted complex trapped mode wavenumbers is given in Table 1, which shows the real and imaginary parts of the wavenumber, normalised by column radius, and the associated period and wavelength for the simple four bottom-seated circular columns described above.

The first and lowest mode predicted has a normalised wavenumber of $\mathrm{Re}(ka)=$ 0.324 which for the geometry described above corresponds to an excitation period of 12.38 s. Typical storm waves on the open ocean have a peak period in the range $T_p = 12 - 15$ s. This means that the lowest few modes could be significantly excited linearly. For the higher modes the sea-state would have too little spectral energy for near-trapping to be excited through linear excitation. From a practical point of view, having found the near-trapped mode frequencies at which violent wave-structure interactions are most likely to occur, it is then useful to investigate the mode shapes, as this may lead to identification of the locations within the array where water-deck impact is most likely to occur.

6

Re(ka)	Im(ka)	T (s)	λ (m)
0.324	-0.1605	12.38	239.3
0.521	-0.1936	9.789	148.8
0.711	-0.2002	8.330	109.0
0.858	**-0.0600**	**7.582**	**90.37**
1.209	-0.1697	6.408	64.13
1.447	-0.1475	5.865	53.58
1.831	-0.1176	5.215	42.35
2.106	-0.1201	4.851	36.82
2.558	**-0.0724**	**4.409**	**30.31**
2.798	-0.1686	4.210	27.71
2.895	-0.1903	4.138	26.78
3.298	-0.1023	3.882	23.51
3.561	-0.1678	3.732	21.77

Table 1: Near-trapped wavenumbers for the array of four bottom-seated circular columns.

2.1. Mode shape approximation

A method of approximating the shape of the free surface (termed the response) for a near-trapped mode is presented here. Using the method of Linton and Evans (1990) to predict the near-trapped mode frequencies for arrays of cylinders, the associated mode shapes can be obtained based on series expansions. For more general multi-column configurations such as semi-submersibles, an alternative approach is desirable. The near-trapping frequencies may be obtained by observing peaks in the plots of characteristic parameters such as forces or local wave elevations. Having identified the near-trapping excitation frequencies, the corresponding mode shapes may then be approximated using their symmetric and antisymmetric properties. This latter approach is illustrated here. The surface elevation within and around the bottom-seated column array is calculated using the Oxford code DIFFRACT for a unit-amplitude, regular wave train, incident from a single excitation direction. The incident field is

then stripped away to leave the scattered surface response. This calculation is repeated for the same geometry but with the opposite incident wave direction. To save computation time for a symmetric structure, the previously calculated scattered elevation field can simply be mirrored.

For a symmetrical structure, the mode shape will exhibit either symmetry or antisymmetry about an axis running through the geometric centre of the structure perpendicular to the incident wave direction. For example, with the structure discussed above and an incident wave moving broadside from left to right, a symmetrical mode shape with a peak between the two leading columns would also show an equal amplitude peak between the two downstream columns. A mode shape showing antisymmetry would in contrast show a trough between the two downstream columns with a depth equal in amplitude to the height of the corresponding peak. For the next stage in the process, if the mode shape is expected to be symmetric, the two scattered elevation fields from opposing directions are superimposed. If antisymmetric, the same method is used except one subtracts the two scattered fields rather than adding. If rotational symmetry is present then this method can be applied for appropriate pairs of opposing wave directions. Finally, the average of the combined field is taken to give the symmetric or antisymmetric components of the near-trapped mode response.

Figure 2 shows the final stage of the above method for a near-trapped mode with wavenumber $ka = 1.209$ ($T = 6.408$ s) and the appropriate symmetries to be excited by an incident wave direction $\beta = 0\,^{\circ}$ (or $\beta = 180\,^{\circ}$). The direction $\beta = 0\,^{\circ}$ represents waves incident from the left, advancing in the positive x-direction, and β increases with anticlockwise rotation from this direction. This sea state was chosen to linearly excite a near-trapped mode. The final stage is where the two scattered fields from opposite directions can be added or subtracted before being averaged (i.e. divided by $2N_{Pairs}$ where N_{Pairs} is the number of pairs of opposing wave directions) to find the symmetric or antisymmetric components of the mode shape respectively. Figure 2 compares the modulus of the symmetric and antisymmetric components of the mode shape to determine which captures the near-standing wave pattern within the obstacle
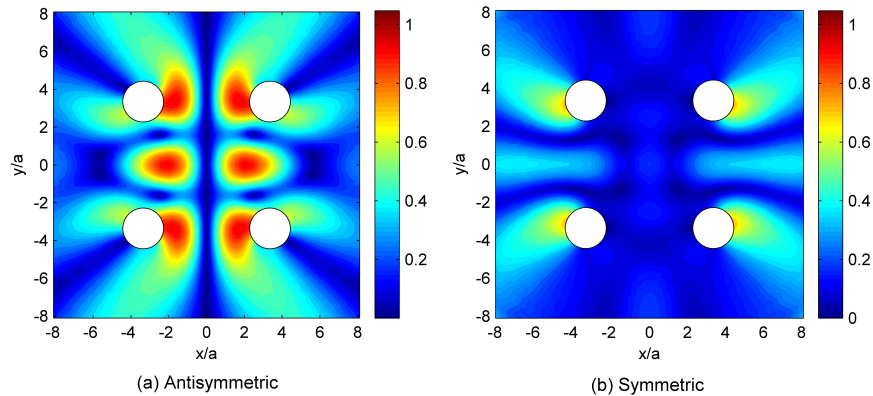
8

array.

Figure 2: Comparison of normalised symmetric and antisymmetric diffraction patterns for first order excitation of a near-trapped mode with four bottom-seated circular columns and ω=0.980 rad/s ($T = 6.408$ s), $\beta = 0\,^\circ$.

Figure 2(a) shows the antisymmetric component and Figure 2(b) shows the symmetric component. Figure 2(a) clearly shows the mode shape with a complicated local 3×2 arrangement of peaks and troughs. This 3×2 pattern is antisymmetric about the vertical axis and so the central peak to the left of the centre is down while the corresponding reflected peak is up forming a $\begin{pmatrix} + & - \\ - & + \\ + & - \end{pmatrix}$ excitation pattern. In contrast, Figure 2(b) shows almost no response within the array for the symmetric case. Thus, the mode shape is antisymmetric about the vertical axis (y), but symmetric about the horizontal axis (x) through the centre.

The method presented above can be applied to each predicted near-trapped mode, regardless of excitation being through first or second order interactions. The modes should be viewed as a mixture of both standing waves and outward propagating radiation because they are not pure trapped modes. Within the array the mixture is mostly standing wave and outside the array it is mostly radiation. These outward propagating components correspond to the radiation damping of the mode. As mentioned above, the size of the imaginary part of the predicted near-trapped wavenumber indicates the amount of damping
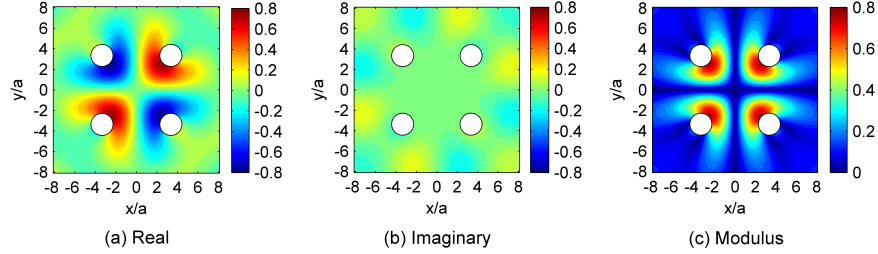
9

within the mode.

Figure 3: Mode shape for a near-trapped mode with four bottom-seated circular columns and ka=0.858 ($T = 7.582$ s), $\beta = 45\,^{\circ}$.

Figures 3 and 4 show the normalised responses in the two modes with the smallest imaginary wave components, $ka = 0.858$ ($T = 7.582$ s) and $ka = 2.558$ ($T = 4.409$ s) respectively. Both modes can be excited by a wave direction of $\beta = 45\,^{\circ}$ and are highlighted in bold in Table 1. Both responses were found using the approximate method and show first order excitation field plots of the real and imaginary components of the response, and the modulus of these. Linear excitation of these mode shapes was discussed in Grice et al. (2013) but the figures have been reproduced here to allow comparison with the eigenvalue method in Section 2.2 and with second order excitation in Section 2.3. Figure 3 is an antisymmetric mode which is symmetric about the diagonal axes but antisymmetric about the x and y axes in an $(\mp\pm)$ excitation pattern. Figure 4 is a symmetric mode with symmetry about the diagonal, x and y axes. The mode shape cannot be described as easily as the previous case but perhaps has an approximate $\begin{pmatrix} + & - & + \\ - & + & - \\ + & - & + \end{pmatrix}$ excitation pattern in the centre region with the outer diagonal elements very close to the columns.

The amplitude (modulus) patterns are helpful for indicating symmetry or anti-symmetry within and outside the array. In contrast, the real and imaginary components indicate the $(+,-)$ checkerboard pattern.
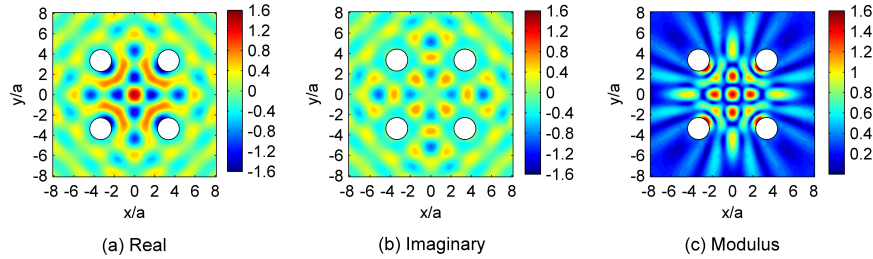
10

Figure 4: Mode shape for a near-trapped mode with four bottom-seated circular columns and $ka = 2.558$ ($T = 4.409$ s), $\beta = 45\,^{\circ}$.

2.2. Eigenvalue method

An alternative and more sophisticated method of predicting the response shape at a near-trapped mode is discussed in Section 3 of Meylan and Eatock Taylor (2009). This is suitable when the set of equations describing the wave-structure interactions can be found using a semi-analytical method, as in Evans and Porter (1997). An eigenanalysis can be performed on these equations, and the resulting eigenvectors are then used with the corresponding eigenvalue to evaluate the surface elevation around the structure for a near-trapped mode. These field plots are used to validate the approximate method discussed in the previous section.
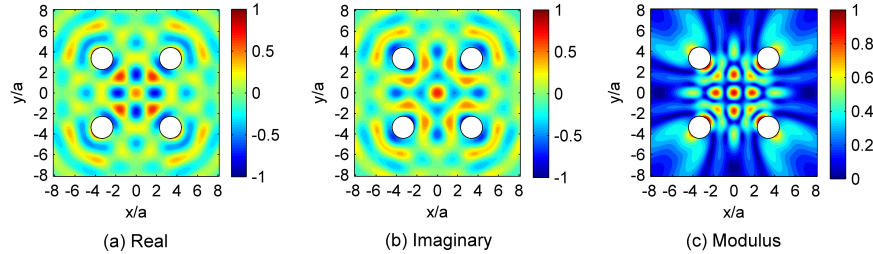

Figure 5: Mode shape (using method of Meylan and Eatock Taylor (2009)) for a near-trapped mode with four bottom-seated circular columns and $ka=2.5576+0.07239$i.

Figure 5 plots the predicted mode shape for a complex wavenumber of $ka=2.5576+0.07239$i. This is the expected mode shape associated with the near-trapped mode using the complex wavenumber as predicted by the method

11

of Linton and Evans (1990), see Table 1. Figures 5(a-c) show the resulting real and imaginary components, and the modulus of these mode shape responses, respectively. Now the numerical method upon which DIFFRACT is based can only analyse wave-structure interactions for real wavenumbers. Figure 6 therefore shows the equivalent eigen analysis mode shape response using the semi-analytical solution evaluated with just the real part of the wavenumber for the near-trapped mode. This allows a more consistent comparison between the two methods. Comparing these plots with those of Figure 4, obtained using the method described in the previous section, shows a good match between the two methods, with just a phase difference. For the approximate method, phase can be defined with respect to the unit amplitude incident wave. In contrast for the complex eigenvalue approach phase in time is arbitrary. There are some differences in the radiating pulses outside the array but within the centre the patterns from the two methods are very close.

(a) Real   (b) Imaginary   (c) Modulus
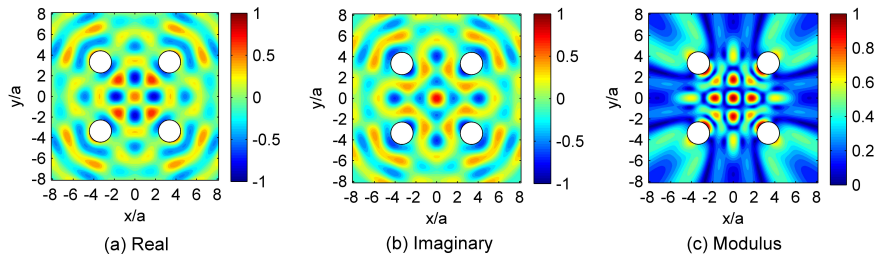
Figure 6: Mode shape (using method of Meylan and Eatock Taylor (2009)) for a near-trapped mode with four bottom-seated circular columns and ka=2.5576 ($T = 4.409$ s).

2.3. Second order mode shapes

The near-trapping phenomenon for arrays of closely spaced columns and methods of predicting their associated mode shapes have been presented above for linear incident waves. In practice, however, only one of the thirteen lowest near-trapped modes predicted could be significantly excited linearly by a typical storm wave. The predicted near-trapped modes are almost all shorter than the typical 12-15 s range of storm peak periods. Since, however, second order

interactions lead to a response at half the incident wave period, several of the identified modes could be significantly excited at second order by typical storm waves.

In this section, comparisons are made between the shapes of modes that are excited linearly and through second order interactions. The aim of this comparison is to determine whether linear calculations, that are quick and cheap computationally, can be used to predict the shape of responses at second order, which are far more computationally intensive. The modes that were excited linearly in the previous section are now excited for the same structure through second order interactions and the results are compared. The linearly excited field plots are normalised by the incident wave amplitude as before, η/A, and the second order excitation field plots will be normalised by $\eta/(kA^2)$, where k is the incident wavenumber and A is the incident wave amplitude.

Incident waves with angular frequencies equal to half those of the linear cases were used. For a second order sum response to these new incident waves, frequency doubling would lead to an excitation at the same response frequency as the identified near-trapped modes. Since modes can be driven by either linear or second order excitation, a detailed comparison is made using the mode from the first case looked at in the previous section (Figure 2) which was excited linearly by an incident wave of ω=0.980 rad/s, $\beta = 0°$. Second order excitation by incident waves of ω=0.490 rad/s ($T = 12.816$ s), $\beta = 0°$ would lead to a response at the same frequency as the first case, ω=0.980 rad/s ($T = 6.408$ s).

Figure 7 compares the symmetric and antisymmetric components of both the first and second order excitation of this mode. For this second order case it is less obvious as to whether a symmetric or antisymmetric standing wave dominates. Figures 7(c) and 7(d) show the antisymmetric and symmetric components respectively with both having complicated response patterns within the array. On first glance it appears that a combination of the antisymmetric and symmetric components would generate a pattern very similar to that excited linearly in Figure 7(a). Figure 7(c) seems closer to the linear pattern than the symmetric Figure 7(d) but the symmetric plot has a 50 % larger maximum

13

response than the antisymmetric plot.

Given the antisymmetric nature of the mode shape when excited linearly, perhaps Figure 7(d) represents some excitation of a different mode. This separate symmetric mode that is driven by second order, but not linear, excitation is "roughly speaking" a completely axi-symmetric ring mode that could be driven by second order excitation from any opposing pair of incident wave directions. One of the reasons that makes this method approximate is that all modes are excited to some extent by an incident wave and so the method is reliant on the response at the peak frequency being sufficiently dominant to render any

(a) First order antisymmetric

(b) First order symmetric

(c) Second order antisymmetric
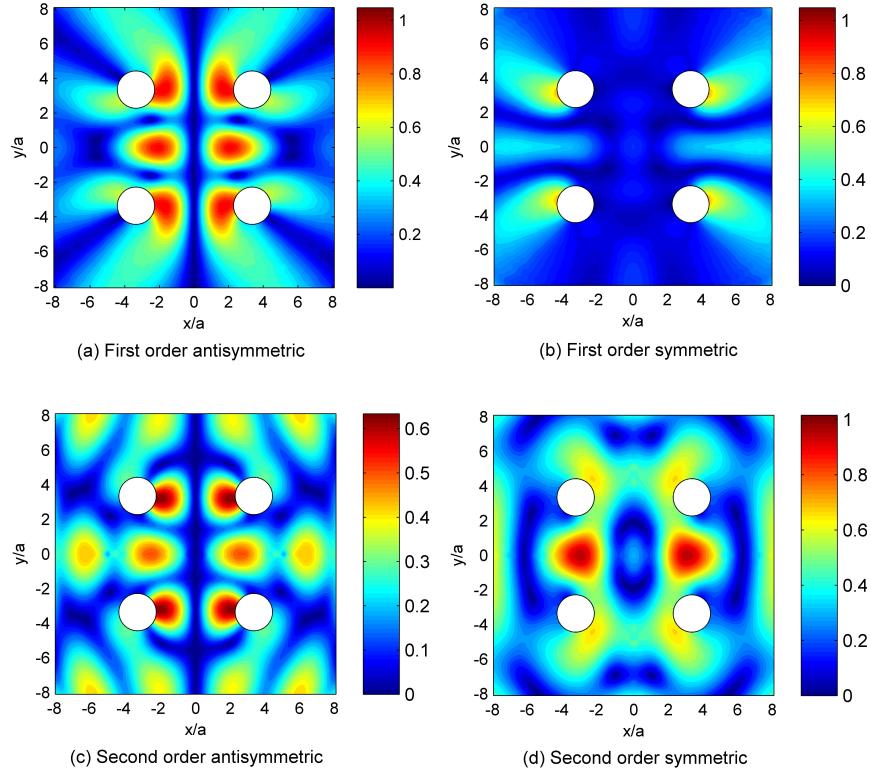
(d) Second order symmetric

Figure 7: Comparison of symmetric and antisymmetric diffraction patterns for a near-trapped mode with first and second order excitation and four bottom-seated circular columns for a response angular frequency ω=0.980 rad/s ($T = 6.408$ s), $\beta = 0\,^{\circ}$.

14

responses due to modes with peak responses at other frequencies negligible.

Figure 8 compares the modulus field plots of linear and second order excitations of four near-trapped mode shapes, all of which can be excited with incident angles of $\beta = 45°$. The four pairs of plots represent modes with response angular frequencies increasing by approximately 0.2 rad/s for each pair, starting and ending with the two modes discussed previously that have the smallest predicted imaginary wavenumber component. Looking at just the linear responses, Figure 8(a,c,e,g), there is a clear progression in the mode patterns as frequency increases. This is to be expected as they are all exciting a standing wave within the same geometry but for decreasing wavelengths.

The first pair of figures, 8(a & b), compare the modulus of the mode shape with the smallest imaginary component in Table 1, $\omega = 0.829$ rad/s ($T = 7.582$ s), with linear and second order excitation respectively. They both show a very similar ($\mp\pm$) oscillating pattern, and within the array the two mode shapes are almost identical. The main differences are in the radiation moving out from the array. The linear case, 8(a), has boomerang shaped peaks about each column with the ends of two of these extending out to infinity. The second order case, 8(b), shows that the peaks have changed shape with little sheltering behind each column.

When looking at the other first and second order excitation pairs, there are definite similarities between each pair of plots but the level of similarity decreases with frequency. This is also to be expected given the highly complicated nature of the mode shapes at the higher frequencies. For the lowest frequency near-trapped modes, linear calculations can give a good prediction of the second order sum response pattern for arrays of circular columns.

3. Near-flat QTF matrix approximation

Section 2 presented methods for predicting near-trapped mode frequencies and the mode shapes associated with each. It was shown that for the lowest few modes, the mode shape is dependent only on the response frequency,

15

(a) 1st order, ω_I=0.829 rad/s

(b) 2nd order, ω_I=0.414 rad/s

(c) 1st order, ω_I=1.072 rad/s

(d) 2nd order, ω_I=0.5036 rad/s

(e) 1st order, ω_I=1.205 rad/s

(d) 2nd order, ω_I=0.602 rad/s

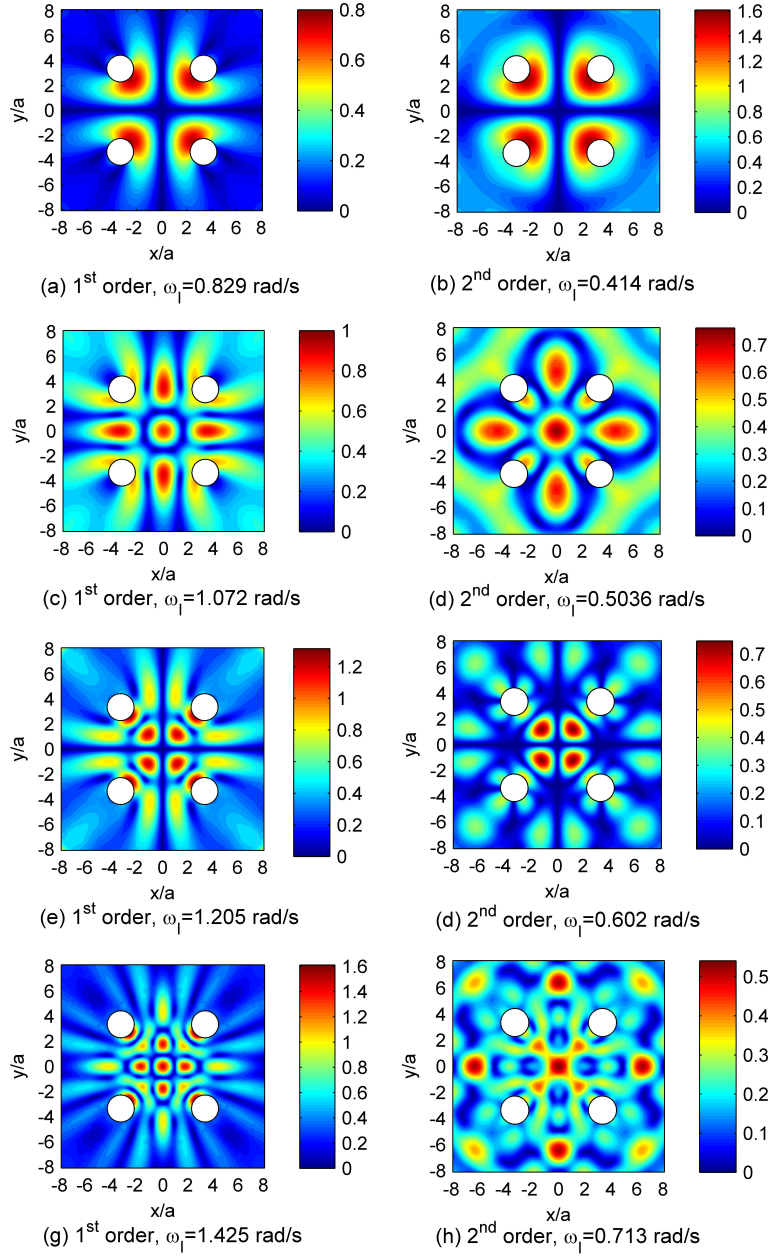(g) 1st order, ω_I=1.425 rad/s

(h) 2nd order, ω_I=0.713 rad/s

Figure 8: Comparison of first and second order excitation of mode shapes for near-trapped modes of increasing incident frequency, ω_I, with four bottom-seated circular columns, $\beta = 45\,^\circ$.

16

and so linear results could be used to estimate the shape of the near-trapped modes driven by second order excitation. However, this did not hold for higher frequency mode shapes. In addition to this, Section 2 only looked at monochromatic cases, but for realistic modelling of extreme wave-structure interactions a real sea-state with a broadbanded spectrum should be used. A broadbanded spectrum with N components leads to an $N \times N$ matrix of QTFs, each entry of which requires a lengthy calculation. A method of minimising the number of computationally intensive QTF calculations required to accurately model second order wave-structure interactions would therefore be very useful. This section discusses an approximation to the QTF matrix using the hypothesis that for the first few modes QTFs are defined by the sum response frequency and that the difference frequency has a negligible influence on the interaction.

Taylor et al. (2007) introduced an approximation to the QTF matrix based on this assumption that QTFs are dependent on the response frequency far more than the difference frequency. In a three dimensional plot of a QTF (e.g. modulus) versus the two incident wave frequencies (ω_i, ω_j) , the QTF is therefore approximately flat perpendicular to the leading diagonal. A summary is given here of the explanation in Taylor et al. (2007) as to why the QTF matrix (corresponding to discrete frequencies) can be approximated in this way. For a pair of incident waves, with amplitudes (A_i, A_j), a sum frequency QTF matrix H with elements H_{ij} can be found that will give the second order sum surface elevation in terms of these incident linear wave components as:

$$\eta^{(+)}(x,y) = H_{ij}(x,y)A_i A_j e^{i\Omega^+ t} \tag{3}$$

where the QTF is a function of the location relative to the array geometric centre $(x = 0, y = 0)$ and $\Omega^+ = (\omega_i + \omega_j)$ is the sum or output frequency. The frequency difference is given by $\Omega^- = (\omega_i - \omega_j)$, and in the QTF matrix is equal to the distance away from the leading diagonal of the matrix.

The second order sum response from Equation 3 contains a potential term and a quadratic term, of which the potential term dominates (see Walker et

17

al. (2008)). This potential sum term can itself be separated into two parts: the scattering from the incoming bound second order sum potential and the part driven by the free-surface integral. The free-surface integral contribution can be defined as the solution to Laplace's equation subject to the free surface boundary condition given in Equation 4 (see for example Garrison (1984)).

$$\frac{\partial \phi^+}{\partial z} - \frac{(\Omega^+)^2}{g}\phi^+ = f^+(x,y) \tag{4}$$

The source term, $f^+(x,y)$ is simply a set of products of linear wave components at frequencies ω_i and ω_j. An integral solution for the potential is given by Equation 5, where the first two integrals are over the body surface and the third integral is over the free-surface.

$$2\pi\phi^+ + \int \phi^+ \frac{\partial G}{\partial n}dS_B - \int G\frac{\partial \phi^+}{\partial n}dS_B = \int Gf^+dS_F \tag{5}$$

$G(\Omega^+)$ is a linear Green's function, which is a function of Ω^+, hence changes to the (ω_i, ω_j) pair have no effect on $G(\Omega^+)$ as long as the sum frequency $\Omega^+ = (\omega_i + \omega_j)$ remains constant. If the major contribution to the QTF which is associated with ϕ^+ varies with frequency pair (ω_i, ω_j) while keeping Ω^+ constant, then these changes must be due to variations in the source term.

At low frequencies, where the wavelengths of the linear incident waves are long relative to the array geometry, there is little diffraction and there are no significant differences between the response and incident fields. Therefore, at these low frequencies there can be little variation across the array in the product source terms, $f^+(x,y)$. Thus, at low frequencies neither the Green's function or the source term are strong functions of $\Omega^- = (\omega_i - \omega_j)$ when $\Omega^+ = (\omega_i + \omega_j)$ is fixed. As these components of the potential sum terms are the solution to the integral equation driven by the free-surface integral, their contribution to the QTFs cannot vary significantly with the distance from the leading diagonal, Ω^-. For second order sum excitation of the first few near-trapped modes there can be a large second order response while satisfying the requirement of the incident wavelengths being long relative to the structure.

The free-surface integral part of the second order sum response has been discussed but there is still a contribution from the scattering of the incoming bound second order sum potential. Since the sum frequency term, Ω^+, determines the efficiency of scattering then the difference frequency, Ω^-, is likely to have little effect on the scattered field for each frequency pair with the same Ω^+. This requires that the column array dimensions are fairly small relative to the wavelengths corresponding to k_i or k_j, the wavenumbers of the incident waves giving rise to the second order sum component. Looking back to Table 1, one sees that the final column shows the wavelengths at each near-trapped mode. Due to the squared relationship between wavenumber and angular frequency (at least in deep water), the wavelength of an incident component that would lead to monochromatic second order sum excitation of a near-trapped mode would be four times that associated with the response mode as given in the table. This means that the first three or four modes corresponding to near-trapping at $(\omega_i + \omega_j)$ could satisfy the requirement that the column array dimensions be fairly small relative to the wavelengths corresponding to ω_i or ω_j.

3.1. QTF structure

To assess the usefulness of this near-flat QTF approximation, results will be presented based on a more realistic model of a large offshore platform (a semi-submersible in water of depth 300 m, see Figure 1(b)) than the simplified model used so far, Figure 1(a). The geometry consists of four columns located at $(\pm 41.42 \text{ m}, \pm 41.42 \text{ m})$ and four pontoons connecting the columns beneath the free surface. The total draft of the structure is 30 m, the pontoons have a height of 11.52 m, and the deck is 17.5 m above mean sea level. The column cross-sectional shape is a square of width 23.4 m with rounded corners of radius 7.68 m, and has the same cross-sectional area as the circular columns used previously in the simplified model. For this assessment of the QTF behaviour, the structure is held fixed. This new model is close enough to the earlier simplified model that the predicted near-trapped mode frequencies shown in Table 1 are approximately those for the new structure.

19

The calculation of QTFs requires a calculation at all the frequency pairs, (ω_i, ω_j), which are needed to model a random sea state realistically. Due to the high computation time of each calculation one should find the minimum number of frequency components required to accurately characterise the QTF behaviour, e.g. $N = 10\text{-}15$, and then interpolate between these if required. One can use symmetry in the QTF structure to reduce the number of calculations from N^2, where N is the number of frequency components in the incident spectrum, to $N(N + 1)/2$. This is because for the second order sum terms, $QTF(\omega_i, \omega_j) = QTF(\omega_j, \omega_i)$, and for second order difference terms, $QTF(\omega_i, \omega_j)$ is the complex conjugate of $QTF(\omega_j, \omega_i)$. If for example $N = 13$, then the number of calculations can be reduced from 169 to 91 with use of the QTF symmetry. The flat-QTF approximation introduced by Taylor et al. can then reduce this even further to just 13 calculations. Figures 9 and 10 plot the actual QTFs for the typical large semi-submersible discussed above, as calculated using the computer program DIFFRACT.

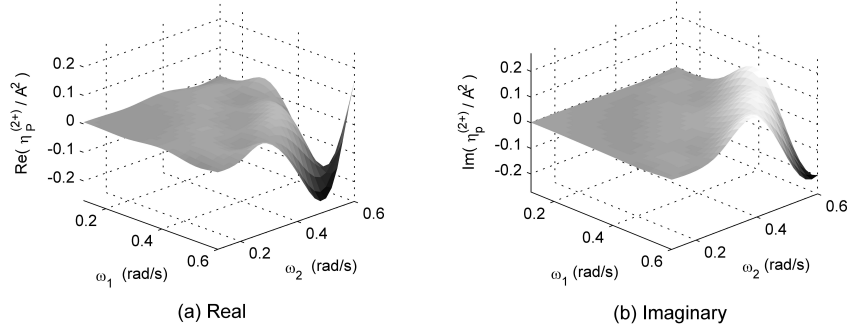(a) Real   (b) Imaginary

Figure 9: Components of the potential sum surface elevation QTFs against higher incident frequencies with $0.12 \leq \omega_i, \omega_j \leq 0.6$ rad/s, $\beta = 45°$, and $x = 12$ m, $y = 12$ m.

Figure 9 shows the real and imaginary components of the potential sum QTF for each pair of incident frequency components in the range $0.12 \leq \omega_i, \omega_j \leq 0.60$ rad/s for a wave direction of $\beta = 45°$ diagonally across the structure. The QTFs are calculated at the location (12 m,12 m) within the array, where the origin is at the array centre. This location was chosen as it is known to give

large responses at certain near-trapped modes, including the $T = 7.582$ s mode shown in bold in Table 1 as being likely to produce a violent response. This mode should be excited at second order within the range of frequencies covered in Figure 9. Plotting the components shows clearly a ridge of high amplitude running perpendicular to the leading diagonal at a response frequency around 0.85 rad/s corresponding to the near-trapped mode of $T = 7.582$ s. There is perhaps another less obvious excitation of a near-trapped mode at the lower response frequency of 0.75 rad/s which matches a near-trapped mode at $T = 8.330$ s. Within the frequency range shown it is clear that assuming QTFs are flat perpendicular to the leading diagonal is a reasonable approximation.

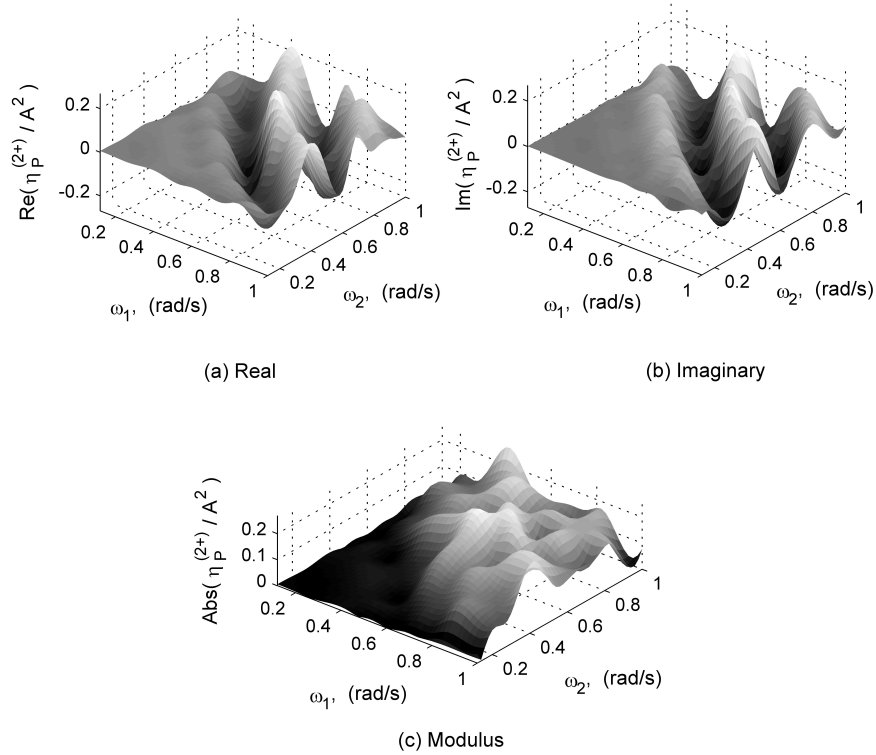

(a) Real

(b) Imaginary

(c) Modulus

Figure 10: Components of the potential sum surface elevation QTFs against higher incident frequencies with $0.12 \leq \omega_i, \omega_j \leq 1$ rad/s, $\beta = 45°$, and $x = 12$ m, $y = 12$ m.

Figure 10 now extends the range of frequencies covered to $0.12 \leq \omega_i, \omega_j \leq 1$

rad/s for the real and imaginary components, and the modulus of these, of the potential sum QTF. It is immediately clear that at the higher frequencies there is more variation perpendicular to the leading diagonal. However, there are still very distinct ridges in the real and imaginary components showing a further two near-trapped modes being excited at response frequencies around 1.4 rad/s and 1.8 rad/s. The 1.4 rad/s near-trapped mode matches well with the 5.215 s mode identified for the structure and the 1.8 rad/s mode goes beyond the near-trapped mode predictions made earlier. The approximation of assuming flat QTFs perpendicular to the leading diagonal is clearly less accurate at higher frequencies, but it can still offer a reasonable alternative to the lengthy process of calculating the full QTF matrix.

It has been shown so far that for low frequencies and the large offshore structure geometry, the surface elevation QTFs for wave-structure interactions were approximately constant close to but perpendicular to the leading diagonal. Further away from the leading diagonal and at higher frequencies this approximation becomes less reliable but a JONSWAP wave spectrum (Hasselmann et al. (1973)) has a high concentration of energy around the peak frequency. For second order responses, the QTFs such as those shown in Figure 10 are used as transfer functions to modify the product of each pair of incident spectral components. By multiplying the incident spectral components, the concentration of energy around the spectral peak is increased and as one moves away from this spectral peak the amount of spectral energy quickly decreases. For an incident JONSWAP spectrum with a peak period of $T = 15.164$ s, the spectral energy decreases quickly away from the peak so that at frequencies 10 % either side of the peak the spectral energy has dropped by approximately 50 %. Further away from the peak there is an '$\times$' shape of increased amplitude along the two lines $\omega_1 = \omega_p$ and $\omega_2 = \omega_p$. At a distance of ω_p from the peak, these lines of increased energy have been reduced to less than 3 % of the peak energy and away from those lines of increased amplitude the spectral energy has been reduced to less than 1 %. The weighting is so strong near the peak frequency that frequency pairs only a short distance away from the peak will have little effect.
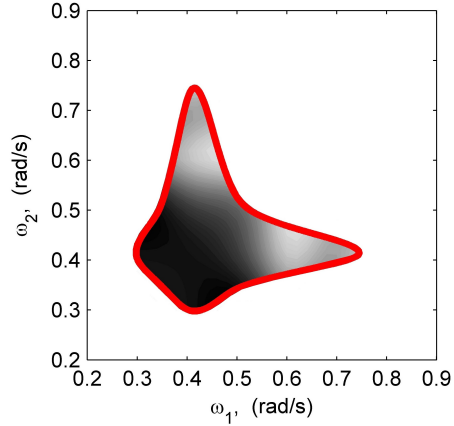
22

Figure 11: Second order potential sum QTFs at frequency pairs with more than 5 % of the maximum spectral energy for an incident JONSWAP wave with a peak period of $T_p = 15.164$ s ($\omega_p = 0.4$ rad/s).

To further illustrate that only the QTFs close to the peak frequency are important, Figure 11 uses the quadratic spectral energy distribution to find the frequency pairs where the spectral contribution is greater than 5 % of the maximum. The potential sum QTF magnitude at (12 m,12 m) from Figure 10 is then plotted at these frequency pairs. The white areas in Figure 11 represent frequency pairs where the spectral contribution is less than 5 % of the maximum value. The shaded areas show contours of the magnitude of the potential sum QTF where the spectral contribution is greater than 5 % of the maximum value. The border plotted along the boundary between these two areas is the contour at which the spectral contribution is equal to 5 % of the maximum value. The number of frequency pairs with more than 5 % of the maximum spectral contribution is fairly small. Most of these pairs are centred about the peak, (ω_p, ω_p), with two extensions of the plotted area along the lines $\omega_1 = \omega_p$ and $\omega_2 = \omega_p$. This suggests that assuming the QTFs are completely flat perpendicular to the leading diagonal can be a useful approximation to save time on the computationally intensive calculation of QTFs if the peak frequency is fairly low. It also shows that when using incident JONSWAP spectra, a cutoff at $\omega_{Max} = 2\omega_p$ can

23

be used without too much loss of spectral energy.

3.2. The effect of QTF approximation

3.2.1. Semi-submersible platform

The approximation of assuming that QTF matrices are flat perpendicular to the leading diagonal has been discussed as a possible method to reduce computation time. To investigate the accuracy of this approximation, a set of 10000 random open-ocean wave elevation spectra were generated corresponding to $H_s = 12$ m and $T_p = 15.164$ s. This peak period was chosen because this is twice as long as the fourth near-trapped mode excitation period. Second order sum responses for this peak period should therefore excite the fourth near-trapped mode. $H_s = 12$ m was selected to give a steep sea state with the chosen peak period. Such an (H_s, T_p) combination is representative of winter storm conditions in the North Sea.

A JONSWAP spectrum was used as the target sea state with the H_s and T_p discussed above, $\gamma = 3.3$, and $N = 1024$ spectral components. For each of the 10000 random open-ocean spectra to be generated a set of $(N \times 2)$ random numbers were produced with zero mean and unit variance. These random amplitudes were then introduced in the spectral domain to modify the JONSWAP spectrum and create a random realisation of the sea state. Every random realisation required $(N \times 2)$ random numbers because there are N spectral components in the target JONSWAP sea state, each of which has a real and imaginary part to be modified by separate random amplitudes. The generation of a large number of relatively short random time histories (3-4 hours) which can then be combined into one large data set was found to be more convenient than the generation of a single long time history of equivalent length. 10000 time histories each of length around 4 hours were generated and combined to give a total data set of over 750000 waves for the chosen sea state, allowing extreme value statistics to be collected without extrapolation.

The 10000 random wave histories represent the undisturbed surface elevation with no structure present. To account for the presence of the large offshore

structure these random open ocean time series were modified using either the full QTF matrix or the assumed flat QTF matrix to give two sets of random response surface elevation spectra. In both, the linear transfer functions were used to account for linear diffraction. Both sets are based on the same realisation of the random undisturbed field. However, there will be differences between the two sets due to some inaccuracies introduced with the flat QTF approximation. Having generated the two sets of random response elevation spectra, the inverse FFT was taken for each random response spectrum to give the associated time history for the response surface elevation in the given sea-state. Every zero-upcrossing location and the crest and trough between each zero-upcrossing were then identified and combined to give two large datasets, each with over 750000 crests, using the full QTF matrix in one set and the flat QTF approximation in the second set. Within each set the crests were ordered in terms of elevation and the largest 500 were isolated and aligned so that all the crests were focused at time $t = 0$ s. The average of these was then taken at each point in time for ± 100 s about the crest focus $t = 0$ s to give the average extreme wave elevation for the given sea-state at a response level of approximately one-in-1500 waves (comparable to the number of waves in a large winter storm).

To improve our understanding of exactly how the flat QTF approximation changes the shape of the second order sum packet, Figure 12 shows the individual linear, second order sum, and total elevation components for the crest focused case with the full QTF matrix results shown by the thick line and the flat QTF results shown by the thin line. The total elevation to second order in the presence of the structure (Figure 12(b)) shows that the shape of the packet is very similar between the two signals, with the full QTF matrix producing a maximum amplitude of 21.35 m and the flat approximation set producing a maximum amplitude of 21.94 m. This is just a 2.8 % difference between the two in what is a reasonably steep sea-state. This 2.8 % difference is purely due to the QTF approximation as the same random linear time signal is used in both the full QTF and flat QTF datasets. There are, however, some obvious differences between the two signals, particularly at the troughs either side of the
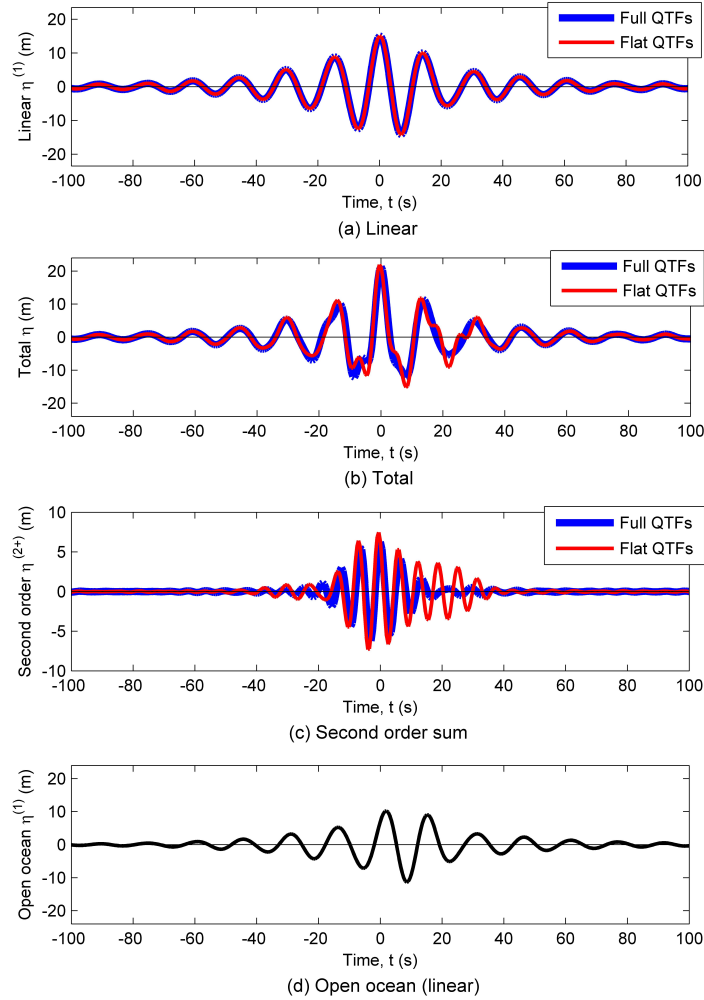
Figure 12: (a) Linear, (b) total, (c) second order sum components of the average of the surface elevation for the largest 500 peaks in the presence of a structure with $H_s = 12$ m, $T_p = 15.164$ s for a full QTF matrix (thick line) and a flat QTF matrix (thin line). (d) is the linear component of the open ocean surface elevation without the presence of the structure.

largest crest. The differences between the two signals quickly become negligible after a few periods either side of the main crest, which is to be expected since the differing second order packets will be fairly compact.

The flat QTF second order sum component has an increased maximum amplitude of 7.47 m, compared to 6.28 m for the full QTF component (Figure 12(c)). The packet is also less compact in time than the equivalent full QTF signal with larger amplitude oscillations in the flat QTF signal between 15-35 s after the focus time. Overall these results show that for this sea-state the flat QTF approximation gives a fairly good approximation of the largest total maximum elevation reached for a given number of waves but the approximation of the complete time history of the second order component itself is less good. Despite this the flat QTF approximation may be useful in 'screening' possible design modifications to reduce water projection to high levels.

The final time history, Figure 12(d), corresponds to the linear input undisturbed average time history for the responses shown above. This plots the free-field conditions (i.e. if the structure were not present) required to produce these high responses.

3.2.2. Single Column

To further investigate the effect on solution accuracy of using the flat-QTF approximation, comparisons were made between reconstructions of experimental data using full and approximate QTF matrices for a simpler structure of a single surface-piercing circular column. Having seen in the previous example that the flat QTF approximation is useful for a case where there is a plethora of near-trapped modes, we now turn to a single column geometry where there are no near-trapped modes but where we have experimental data. Data were obtained from experiments conducted at DHI (www.dhigroup.com), for interactions of focused wave groups with a single circular column of diameter $D = 0.25$ m in water of depth $h = 0.505$ m. The example discussed in this section is a focused incident wave group based on a JONSWAP spectrum with peak period $T_p = 1.63$ s truncated at a frequency 4.1 times the spectral peak, $k_p A = 0.2$,

and $A/D = 0.46$, where k_p is the peak wavenumber, and A is the incident wave amplitude.

Froude scaling can be used to show that experimental results from the single column with $T_p = 1.63$ s would be similar to any wave-structure interactions if just one of the four columns from the previous structure was isolated in the $T_p = 15.164$ s sea state. There is a scaling factor of approximately 100 for the column diameters with values of 0.25 m and 24.6 m respectively. The period will therefore scale by $100^{\frac{1}{2}}$, which is close for the respective periods of 1.63 s and 15.16 s. A single column from the four-column array discussed earlier is therefore very similar to the isolated DHI column from the experimental data. However, the four-column case experienced near-trapped mode excitation whereas for the isolated column there are no near-trapped modes to excite.

Measurements were taken of the time histories for both the incident surface elevation and the force on the column. Linear and quadratic transfer functions were calculated with DIFFRACT to allow the reconstruction of the hydrodynamic force time history from the measured incident surface elevation. This reconstructed force time history was found using both the full QTF matrix and the flat QTF approximation, and both solutions were compared against the measured force time history. For more information on these experiments and the hydrodynamic force reconstruction see Zang et al. (2010).
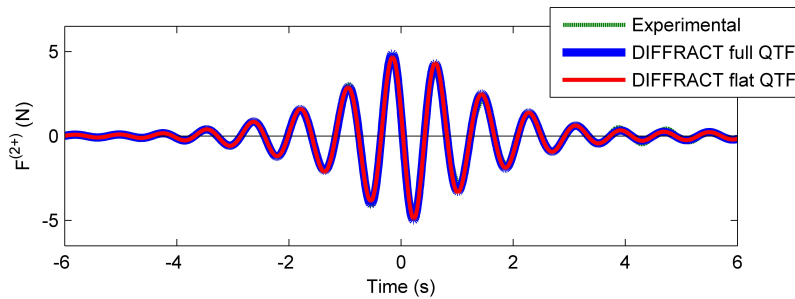

Figure 13: Second order potential sum QTFs at frequency pairs with more than 5 % of the maximum spectral energy for an incident JONSWAP wave with a peak period of $T_p = 15.164$ s.

Figure 13 compares the experimental and reconstructed second order sum component of the hydrodynamic force. The dashed line plots the experimental results, the thin solid line plots the reconstruction found using the flat-QTF approximation, and the thick solid line plots the reconstruction found using the full QTF matrix. There is very little difference between the flat QTF approximation and the full QTF matrix results. The flat QTF approximation leads to a small reduction in amplitude at the largest peaks and troughs relative to the full matrix results but overall the two time histories match far more closely than the second order sum component in the previous semi-submersible wave surface elevation example, with the excitation of many near-trapped modes. More detailed analysis of the experimental results is presented in Fitzgerald et al. (2014).

Our theoretical argument as to why the sum component QTF matrix appears approximately flat in the difference frequency direction relies on features of the sum frequency Green's function and the excitation. In addition, for a simple structure without near-trapped modes, both the Green's function and the second order excitation are unlikely to vary quickly in the sum frequency direction, so it should not be surprising that the flat QTF approximation also holds here.

4. Conclusions

Extreme wave-structure interactions are investigated for a large offshore structure. Near-trapped mode shapes were compared for first and second order excitation using quadratic transfer functions to find the second order surface elevations. An efficient approximation was then investigated to minimise the computation time associated with finding the QTFs.

A simple method for finding near-trapped mode shapes using symmetry and anti-symmetry in wave fields from opposing incident directions was shown to give a good approximation relative to more complex and elegant methods (which are only likely to be suitable when analytical solutions are available) with minimal computation time. Second order diffraction patterns were compared to linear

results and it was found that the diffraction pattern was similar for second order double frequency excitation to the linear behaviour at the same response frequency. For the simple geometry of four circular columns one can use linear results to give reasonable approximations of low frequency near-trapped mode shapes excited by second order sum interactions. At higher frequencies the second order and first order mode shapes become less similar.

It has been shown here that in long waves one can approximate the QTF sum-interaction matrices as being flat perpendicular to the leading diagonal. This allows the number of lengthy second order calculations necessary $(N(N+1)/2)$ to be reduced to just N along the leading diagonal. At higher frequencies there is more variation and a flat QTF approximation becomes less accurate.

Comparison of surface elevation time histories and hydrodynamic force time histories calculated using both the full QTF matrix and the flat QTF approximation showed that the results for the approximation were fairly close to the full matrix solutions. This has demonstrated that the flat QTF approximation can be used to greatly reduce the number of lengthy QTF calculations needed for second order solutions without significantly compromising the quality of results. The approach worked for both a large semi-submersible geometry, where near-trapped mode excitation is important, and for a single compact column in fairly shallow water, where no near-trapped modes exist. This suggests that the flat-QTF approximation is quite generally applicable at low wave frequencies.

Acknowledgements

References

Eatock Taylor, R. (1991) Assessment of springing in tension leg platforms. In Advances in Marine Structures II, ed. C.S. Smith and R.S. Dow, Publ. by Elsevier Applied Science, p174-207.

Eatock Taylor, R. and Chau, F.P. (1992) Wave diffraction theory - some developments in linear and non-linear theory. Transactions of ASME, Journal of Offshore Mechanics and Arctic Engineering, Vol. 114, p185-194.

Eatock Taylor, R., Taylor, P.H., and Sun, L. (2008) Efficient second order diffraction method for multiple bodies in waves. SAFE OFFLOAD Report.

Evans, D.V., Levitin, M., and Vassiliev, D. (1994) Existence theorems for trapped modes. Journal of Fluid Mechanics, Vol. 261, p21-31.

Evans, D.V. and Porter, R. (1997) Near-trapping of waves by circular arrays of vertical columns. Applied Ocean Research, Vol. 1187, p83-99.

Fitzgerald, C., Taylor, P.H., Eatock Taylor, R., Grice, J.R., and Zang, J. (2014) Phase manipulation and the harmonic components of ringing forces on a surface-piercing column. Proc. Royal Society of London Series A - Mathematical Physical and Engineering Sciences, Vol. 470, no. 2168, 20130847.

Garrison, C. J. (1984) Nonlinear wave loads on large structures. Proc. 3rd International Offshore Mechanics and Arctic Engineering Symp., Vol. 1, p128-135, American Society of Mechanical Engineers.

Grice, J.R., Taylor, P.H., and Eatock Taylor, R. (2013) Near-trapping effects for multi-column structures in deterministic and random waves. Ocean Engineering, Vol. 58, p60-77.

Grice, J. (2013) Prediction of extreme wave-structure interactions for multi-columned structures in deep water. D.Phil thesis, University of Oxford.

Hasselmann, K., Barnett, T.P., Bouws, E., Carlson, H., Cartwright, D.E., Eake, K., Euring, J.A., Gicnapp, A., Hasselmann, D.E., Kruseman, P., Meerburg, A., Mullen, P., Olbers, D.J., Richren, K., Sell, W., and Walden, H. (1973) Measurements of wind-wave growth and swell decay during the joint North Sea wave project (JONSWAP). Ergänzungsheft zur Deutschen Hydrographischen Zeitschrift Reihe, Vol. 8(12), p1-95.

Kim, M.H. and Yue, D.K.P. (1990) The complete second-order diffraction solution for an axisymmetric body. Part 2. Bichromatic incident waves and body motions. Journal of Fluid Mechanics, Vol. 211, p557-593.

Lee, C.-H., Newman, J.N., Kim, M.-H., and Yue, D.K.P. (1991) The computation of second order wave loads. OMAE Conference, Stavanger, Norway, Publ by ASME, Vol. 1, Part A, p113-123.

Linton, C.M. and Evans, D.V. (1990) Interaction of waves with arrays of vertical circular cylinders. Journal of Fluid Mechanics, Vol. 215, p549-569.

Linton, C.M. and Evans, D.V. (1993) The interaction of waves with a row of circular cylinders. Journal of Fluid Mechanics, Vol. 251, p687-708.

Meylan, M.H. and Eatock Taylor, R. (2009) Time-dependent water-wave scattering by arrays of cylinders and the approximation of near trapping. Journal of Fluid Mechanics, Vol. 631, p103-125.

Newman, J.N. (1974) Second order slowly varying forces on vessels in irregular wave. Paper 19, pages 182-186 in The Dynamics of Marine Vehicles and Structures in Waves, ed. Bishop, R.E.D. and Price W.G., Publ. By I.Mech. E, London.

Newman, J.N. and Lee, C.-H. (1992) Sensitivity of wave loads to the discretization of bodies. BOSS 92, 6th International Conference on the Behaviour of Offshore Structures; 7-10 July; London, U.K. Proceedings Publ. by BPP Tech Services Ltd., London, Vol. 1, p50-64.

Schetzen, M. (1980) The Volterra and Wiener theories of nonlinear systems. Publ. by John Wiley and Sons.

Stansberg, C.T. (2014) Nonlinear wave amplification around column-based platforms in steep waves. Proc. 33rd International Offshore Mechanics and Arctic Engineering Symp., San Francisco, USA, Vol. 1, Part B, p46-55.

Taylor, P.H., Zang, J., Walker, D.A.G., and Eatock Taylor, R. (2007) Second order near-trapping for multi-column structures and near-flat QTFs. 22nd IWWWFB, Croatia, `http://www.iwwwfb.org/Abstracts/iwwwfb22/iwwwfb22_48.pdf`.

Walker, D.A.G., Eatock Taylor, R., Taylor, P.H., and Zang, J. (2008) Wave diffraction and near-trapping by a multi-column gravity-based structure. Journal of Ocean Engineering, Vol. 35(2), p201-229.

Zang, J., Gibson, R., Taylor, P. H., Eatock Taylor, R. and Swan, C. (2006) Second order wave diffraction around a fixed ship-shaped body in unidirectional steep waves. Transactions of ASME, Journal of Offshore Mechanics and Arctic Engineering, Vol. 128(2), p89-99.

Zang, J., Taylor, P.H., Morgan, G., Tello, M., Grice, J., and Orszaghova, J. (2010) Experimental study of non-linear wave impact on offshore wind turbine foundations. Proc. 3rd International Conference on the Application of Physical Modelling to Port and Coastal Protection.